Volume 23, No 3 | International Journal of Radiation Research, July 2025

A study on the correlation between histopathological subtypes of solitary invasive pulmonary adenocarcinoma and preoperative CT imaging features

S. Cheng[1], T. Guan[1], L. Zhu[1*], Y. Zheng[1*], F. Li[2]

[1]The General Hospital of Western Theater Command, Chengdu, 610000, China
[2]Southwest Medical University Affiliated Hospital, Luzhou, 646000, China

► ***Original article***

Corresponding authors:
Lingxi Zhu, M.D.,
Yifeng Zheng, M.D.,
E-mail: *qras510@163.com, hddv780@163.com*

Received: April 2025
Final revised: April 2025
Accepted: May 2025

Int. J. Radiat. Res., July 2024; 23(3): 543-549

DOI: 10.61186/ijrr.23.3.5

Keywords: *Adenocarcinoma of lung, lung neoplasms, CT scan, radiomics.*

ABSTRACT

Background: Lung adenocarcinoma exhibits considerable heterogeneity in histological subtypes, which are closely associated with prognosis. This study aimed to investigate the correlation between preoperative chest computed tomography (CT) features and histopathological subtypes of solitary invasive pulmonary adenocarcinoma, with the goal of establishing predictive imaging markers. ***Materials and Methods:*** A retrospective analysis was conducted on 187 patients with solitary invasive pulmonary adenocarcinoma (≤3.0 cm), categorized into three groups based on the 2015 WHO classification: G1 (lepidic predominant, n=77), G2 (papillary/acinar predominant, n=65), and G3 (micropapillary/solid predominant, n=45). CT characteristics—including lesion size, CT attenuation values, ground-glass opacity, solid component ratio, lobulation, spiculation, pleural traction, and vascular signs—were analyzed. Multivariate logistic regression and predictive modeling were used to identify independent imaging predictors for each subtype. ***Results:*** Significant differences were found among the three groups in CT values, lesion size, solid component proportion, spiculation, lobulation, and pleural traction ($p<0.05$). Vascular invasion and air space dissemination were significantly more frequent in G3 ($p<0.001$ and $p=0.009$, respectively). Multivariate analysis identified ground-glass opacity, CT value, burr sign, and lesion size as independent predictors for G1; vascular sign and size for G2; and gender (female), lobulation, and pleural traction for G3. The predictive model for G1 showed excellent diagnostic performance with an AUC of 0.986. ***Conclusion:*** Preoperative CT features correlate significantly with histopathological subtypes of lung adenocarcinoma. Distinct imaging patterns can serve as non-invasive predictors, aiding in preoperative risk stratification and individualized treatment planning for patients with pulmonary nodules.

INTRODUCTION

Lung adenocarcinoma represents the most prevalent histological subtype of non-small cell lung cancer (NSCLC), accounting for nearly 40% of all lung cancer cases globally [1-4]. It is a heterogeneous disease with distinct pathological growth patterns-lepidic, acinar, papillary, micropapillary, and solid-each associated with different biological behaviors, prognoses, and therapeutic responses [5, 6]. In 2011, a joint classification by the International Association for the Study of Lung Cancer (IASLC), American Thoracic Society (ATS), and European Respiratory Society (ERS) was introduced and later adopted by the World Health Organization (WHO) in 2015 to improve prognostic stratification and clinical management of invasive pulmonary adenocarcinoma [7].

Histopathological subtypes have been shown to correlate strongly with patient outcomes. For instance, micropapillary and solid subtypes are considered high-risk due to their aggressive behavior and association with lymphatic invasion and poor survival rates [8, 9]. Conversely, lepidic-predominant adenocarcinomas are often associated with favorable outcomes and lower rates of recurrence [10]. Accurate preoperative identification of these subtypes is therefore critical for optimizing surgical planning and guiding treatment decisions.

Chest computed tomography (CT) is routinely employed in the detection and characterization of pulmonary nodules [11, 12]. Advances in high-resolution CT imaging have enabled the assessment of features such as ground-glass opacity (GGO), solid component proportion, lesion size, lobulation, spiculation, and pleural traction-all of which may reflect underlying tumor histology [13, 14]. Several studies have suggested that these imaging characteristics are predictive of tumor invasiveness and histopathological subtype [13, 15]. For example, Ichinose *et al.* demonstrated that higher CT attenuation values are associated with invasive features in ground-glass nodules [16], while Yoshida *et al.* linked solid nodule appearance on CT with

[DOI: 10.61882/ijrr.23.3.5]

micropapillary and solid subtypes [17].

Despite these advancements, there remains a need for systematic studies correlating CT features with WHO-classified histological subtypes in small (≤3.0 cm), solitary invasive lung adenocarcinomas. Current evidence is limited, and predictive models integrating radiological parameters with histopathology are not yet routinely applied in clinical practice. Furthermore, distinguishing histological subtypes non-invasively remains a challenge, particularly for intermediate-risk groups with mixed features.

This study aims to fill the current gap by evaluating the correlation between preoperative CT imaging features and histopathological subtypes in patients with solitary invasive pulmonary adenocarcinoma. By implementing a detailed set of quantitative and morphological CT parameters, we develop predictive models for WHO-classified subtypes. This also offers a novel, non-invasive framework to improve diagnostic accuracy and guides individualized risk stratification and clinical decision-making in early-stage lung adenocarcinoma.

MATERIALS AND METHODS

Study design and ethics

This was a retrospective observational study conducted at the Thoracic Surgery Department of the Western Theater Command General Hospital between January 2020 and December 2023. The study protocol was approved by the Institutional Ethics Committee of the Western Theater Command General Hospital (Approval No. WTCGH/EC/2020-0143, Date: January 10, 2020). All patient data were anonymized, and the study adhered to the ethical guidelines of the Declaration of Helsinki [18].

Patient selection

A total of 187 patients with solitary invasive pulmonary adenocarcinoma were enrolled. *Inclusion criteria were*: Histologically confirmed invasive adenocarcinoma post-surgical resection; A single pulmonary nodule with a maximum diameter ≤ 3.0 cm on chest CT; Availability of high-quality preoperative CT images acquired within four weeks before surgery; No history of neoadjuvant therapy prior to surgery.

Exclusion criteria included: Presence of multiple pulmonary nodules; Poor image quality or incomplete imaging data; Rare histological subtypes not covered by the 2015 WHO classification.

CT Imaging protocol and analysis

All patients underwent chest CT scans using a Siemens SOMATOM Definition AS+ 128-slice spiral CT scanner (Siemens Healthineers, Germany). Scans were acquired in the supine position during deep inspiration. Parameters included: Tube voltage: 120 kVp; Tube current: 180–250 mAs; Slice thickness: 1.0 mm; Reconstruction interval: 0.6 mm. Images were interpreted by two board-certified thoracic radiologists with ≥10 years of experience, blinded to histopathological outcomes. Imaging features assessed included: Longest nodule diameter; Mean CT attenuation (Hounsfield Units, HU) using GE AW Workstation 4.7 (GE Healthcare, USA); Ground-glass opacity (GGO) component (%); Solid component proportion (%); Lobulation, spiculation, and pleural traction; Vascular and bronchial signs; Air bronchograms, vacuole sign, and cavitation.

Histopathological examination

Surgical specimens were fixed in 10% neutral-buffered formalin and embedded in paraffin. Tissue sections were cut at 4 μm and stained with hematoxylin and eosin (H&E) using standard protocols. Slides were examined under a Nikon Eclipse Ci-L microscope (Nikon Corp., Japan) by two pulmonary pathologists independently, blinded to imaging results. Histological classification followed the 2015 WHO and IASLC/ATS/ERS criteria [22, 23]. The predominant subtype was defined as the component occupying the largest area in a single slide. Cases were categorized as: G1 (Low risk): Lepidic predominant; G2 (Intermediate risk): Acinar or papillary predominant; G3 (High risk): Micropapillary or solid predominant (>5% of either component).

Additional pathological features assessed included: Lymphovascular invasion; Visceral pleural invasion and Spread through air spaces (STAS). Representative histological photomicrographs for each subtype were captured using a Nikon DS-Fi3 camera and are presented in figure 1A–F, with regions of interest marked by arrows.

Radiological figures

Preoperative CT images of representative nodules from each group (G1, G2, G3) are shown in figure 2A-F, with clear annotations (arrows) indicating solid components, GGO, lobulation, and pleural traction. All images were adjusted for optimal resolution using Adobe Photoshop CC 2023 (Adobe Inc., USA) to enhance visual clarity.

Statistical analysis

All statistical analyses were performed using IBM SPSS Statistics v26.0 (IBM Corp., USA). Continuous variables were expressed as mean ± standard deviation and compared using one-way ANOVA. Categorical variables were compared using the Chi-square test. Multivariate logistic regression was used to identify independent predictors of histologic subtype. Predictive models for each subtype group (G1 vs others, G2 vs others, G3 vs others) were constructed. Model performance was evaluated using Receiver Operating Characteristic (ROC) curves. The Area Under the Curve (AUC), sensitivity, specificity,

[DOI: 10.61882/ijrr.23.3.5]

positive predictive value (PPV), and negative predictive value (NPV) were reported. The ROC curve is presented in figure 3, with enlarged font for axis labels and numerical indicators.

RESULTS

Patient characteristics

A total of 187 patients were enrolled and classified into three histological groups: G1 (lepidic predominant, n=77), G2 (acinar/papillary predominant, n=65), and G3 (micropapillary/solid predominant, n = 45). The mean age was 56.07±10.07 years, with no significant difference among the groups (p=0.109). Gender distribution was significantly different (p=0.004), with a higher proportion of females in G1 (70.1%) and more males in G3 (60%). Tumor location also varied significantly across groups (p=0.006) (table 1).

CT imaging characteristics by histological subtype

Significant differences in CT features were observed among the three groups. G3 tumors demonstrated larger lesion size (mean: 2.11±0.68 cm) compared to G1 (1.26±0.31 cm, p<0.001). Ground-glass component was most prominent in G1 (0.77±0.20), while G3 exhibited almost complete solidification (0.03±0.09). CT attenuation values also showed a progressive increase from G1 to G3 (G1: -486.90 HU; G3: 52.31 HU, p<0.001). Spiculation, lobulation, pleural traction, vascular penetration, lymphatic metastasis, and air space dissemination were significantly more prevalent in G3 (all p<0.05). Vacuole and bronchogram signs showed no significant intergroup differences (table 2).

Table 1. Single factor analysis of general data (Inter-group difference test).

Parameter	Total sample (N=187)	Low-risk G1 group (N=77)	Moderate risk G1 group (N=65)	High-risk G3 group (N=45)	c^2/F	*P*
Age	56.07 ± 10.07	54.29 ± 11.29	57.75 ± 9.12	56.71 ± 8.78	2.239	0.109
Sexuality					10.846	**0.004**
Female	112 (59.9)	54 (70.1)	40 (61.5)	18 (40.0)		
Males	75 (40.1)	23 (29.9)	25 (38.5)	27 (60.0)		
Site					14.248	**0.006**
Upper right	48 (25.7)	23 (29.9)	10 (15.4)	15 (33.3)		
Low right	37 (19.8)	12 (15.6)	20 (30.8)	5 (11.1)		
Right middle	31 (16.6)	16 (20.8)	7 (10.8)	8 (17.8)		
Left top	34 (18.2)	14 (18.2)	13 (20.0)	7 (15.6)		
Left bottom	37 (19.8)	12 (15.6)	15 (23.1)	10 (22.2)		

Table 2. Single factor analysis of image data.

Parameter	Total sample (N=187)	Low-risk G1 group (N=77)	Moderate risk G1 group (N=65)	High-risk G3 group (N=45)	c^2/F	*P*
Size	1.70 ± 0.61	1.26 ± 0.31	1.94 ± 0.48	2.11 ± 0.68	57.413	**<0.001**
Grinding glass composition	0.48 ± 0.37	0.77 ± 0.20	0.44 ± 0.32	0.03 ± 0.09	146.575	**<0.001**
CT Number	-256.03 ± 247.63	-486.90 ± 38.62	-196.02 ± 204.03	52.31 ± 16.13	284.228	**<0.001**
Lymphatic metastasis					50.047	**<0.001**
Nil	132 (70.6)	76 (98.7)	32 (49.2)	24 (53.3)		
Find	55 (29.4)	1 (1.3)	33 (50.8)	21 (46.7)		
Proportion of real					55.823	**<0.001**
≤50%	105 (56.1)	59 (76.6)	42 (64.6)	4 (8.9)		
>50%	82 (43.9)	18 (23.4)	23 (35.4)	41 (91.1)		
Lobation					17.082	**<0.001**
Nil	111 (59.4)	54 (70.1)	42 (64.6)	15 (33.3)		
Find	76 (40.6)	23 (29.9)	23 (35.4)	30 (66.7)		
Fin					8.466	**0.015**
Nil	124 (66.3)	42 (54.5)	47 (72.3)	35 (77.8)		
Find	63 (33.7)	35 (45.5)	18 (27.7)	10 (22.2)		
Vacuole					2.558	0.278
Nil	135 (72.2)	56 (72.7)	43 (66.2)	36 (80.0)		
Find	52 (27.8)	21 (27.3)	22 (33.8)	9 (20.0)		
Bronchogram					1.470	0.479
Nil	151 (80.7)	65 (84.4)	52 (80.0)	34 (75.6)		
Find	36 (19.3)	12 (15.6)	13 (20.0)	11 (24.4)		
Pleural traction					7.885	**0.019**
Nil	112 (59.9)	54 (70.1)	38 (58.5)	20 (44.4)		
Find	75 (40.1)	23 (29.9)	27 (41.5)	25 (55.6)		
Penetration of blood vessels					18.227	**<0.001**
Nil	134 (71.7)	46 (59.7)	59 (90.8)	29 (64.4)		
Find	53 (28.3)	31 (40.3)	6 (9.2)	16 (35.6)		
Vascular invasion					54.910	**<0.001**
Nil	149 (79.7)	75 (97.4)	55 (84.6)	19 (42.2)		
Find	38 (20.3)	2 (2.6)	10 (15.4)	26 (57.8)		
Intracavity diffusion					9.356	**0.009**
Nil	146 (73.3)	76 (83.1)	62(72.3)	8 (17.8)		
Find	41 (26.7)	1(16.9)	3 (27.7)	37 (82.2)		
Visceral pleural invasion					3.904	0.142
Nil	130 (69.5)	57 (74.0)	47 (72.3)	26 (57.8)		
Find	57 (30.5)	20 (26.0)	18 (27.7)	19 (42.2)		

[DOI: 10.61882/ijrr.23.3.5]

Comparison of imaging features across subtypes

Analysis of CT characteristics across subtypes revealed statistically significant differences in several imaging features, including nodule size, CT value, ground-glass component, proportion of solid component, lobulation, spiculation, vascular sign, and pleural traction (all $p<0.05$). However, vacuole and bronchial signs did not show significant variation among the groups ($p=0.468$). Notably, vascular invasion and air cavity dissemination were significantly more frequent in the G3 group ($p<0.001$ and $p=0.009$, respectively), indicating their association with aggressive tumor behavior. No significant differences were observed in pleural invasion rates ($p=0.142$) (table 2)

Logistic regression analysis of predictive features

Multivariate logistic regression analysis was conducted to identify independent CT imaging predictors for each histological subtype. The models revealed distinct combinations of imaging features associated with G1, G2, and G3 subtypes. For the G1 (lepidic-predominant) group, the presence of a burr (spiculation) sign was significantly associated (OR=2.322, $p=0.003$), suggesting outward infiltration consistent with early tumor progression. Ground-glass component percentage showed a strong inverse correlation (OR=0.328, $p=0.009$), and lower CT attenuation values (OR=0.112, $p<0.001$) were also significant indicators. Additionally, smaller lesion size independently predicted G1 classification (OR=0.513, $p=0.001$), reflecting the less invasive nature of these tumors. In the G2 (acinar/papillary-predominant) group, vascular sign emerged as a significant negative predictor (OR=0.210, $p=0.003$), while larger lesion size was a strong positive predictor (OR=2.079, $p<0.001$). These findings suggest that intermediate-risk tumors tend to have more substantial growth while maintaining partial vascular characteristics that distinguish them from G3. The G3 (micropapillary/solid-predominant) group was significantly associated with female gender (OR=2.989, $p=0.004$), indicating a possible sex-linked biological predisposition. Morphological features such as lobulation (OR=2.431, $p=0.019$) and pleural traction (OR=2.806, $p=0.006$) were also independent predictors, indicating aggressive tumor behavior and architectural distortion. These parameters correspond to the highly invasive nature of G3 subtypes. Overall, the regression models demonstrated good discriminative ability for differentiating between the histological subtypes based on non-invasive imaging features (tables 3 and 4).

Predictive model development

To predict histological subtypes non-invasively, patients were grouped into G1 (low risk), G2 (moderate risk), and G3 (high risk). Separate binary logistic regression models (G1 vs. non-G1, G2 vs. non-G2, G3 vs. non-G3) were developed using independent predictors identified through stepwise multivariate analysis.

Model performance was assessed using ROC curves, with AUC, sensitivity, specificity, and predictive values calculated to evaluate diagnostic accuracy (Table 4).

Table 3. Multivariate Logistic regression analysis of pathological subtypes.

Peer group	B	SE	Waldc^2	*P-value*	OR	95% CI
G1 group						
Reference						
G2 group						
Intercept	9.898	2.733	3.622	<0.001	1.988	1.389~14.000
CT Number	0.019	0.005	3.757	**<0.001**	2.996	1.009~9.029
Proportion of real	2.840	1.002	-2.832	**0.005**	1.622	1.423~4.020
Lobation	0.598	1.061	-1.506	0.132	1.019	0.025~1.619
Fin	-1.803	1.362	-1.324	0.186	0.473	0.011~2.379
Pleural traction	0.920	0.818	1.124	0.261	1.232	0.505~1.474
Penetration of blood vessels	1.731	1.005	-1.722	0.085	1.872	0.525~2.613
G3 group						
Intercept	6.194	6.955	3.891	<0.001	1.202	1.053~25.411
CT Number	2.115	0.055	6.088	<0.001	2.032	1.807~15.250
Proportion of real	1.145	4.688	2.097	**0.039**	3.355	1.296~5.693
Lobation	0.815	1.490	4.074	**0.001**	2.177	1.217~8.853
Fin	1.400	1.390	2.156	**0.035**	1.417	1.125~2.073
Pleural traction	0.272	1.370	2.388	**0.017**	1.928	1.392~2.405
Penetration of blood vessels	-0.874	1.867	-0.468	0.640	0.067	0.011~3.200

Table 4. Backward stepwise multivariate logistic regression analysis.

Peer group	B	*PV*	OR	95% CI
G1 vs Others				
Fin	3.451	0.003	2.322	1.256~4.362
Size	-9.022	0.001	0.513	0.013~0.891
Grinding glass composition	-3.541	0.009	0.328	0.101~0.413
CT Number	-9.940	<0.001	0.112	0.001~0.215
G2 vs Others				
Vascular signs	-1.563	0.003	0.210	0.075~0.586
Size	0.732	<0.001	2.079	1.379~3.133
G3 vs Others				
Gender (female)	1.095	0.004	2.989	1.428~6.256
Leaf sign	0.888	0.019	2.431	1.156~5.112
Pleural traction	1.032	0.006	2.806	1.346~5.850

Model performance and diagnostic accuracy

Receiver Operating Characteristic (ROC) analysis was performed to evaluate the diagnostic utility of the models. The G1 model demonstrated excellent performance with an AUC of 0.986 (95% CI: 0.967–0.999), sensitivity of 0.974, and specificity of 0.964. The G2 model also showed good discriminative ability (AUC=0.836), while the G3 model achieved moderate performance (AUC=0.721), with a sensitivity of 0.556 and specificity of 0.782 (figure 1 and table 5).

[DOI: 10.61882/ijrr.23.3.5]

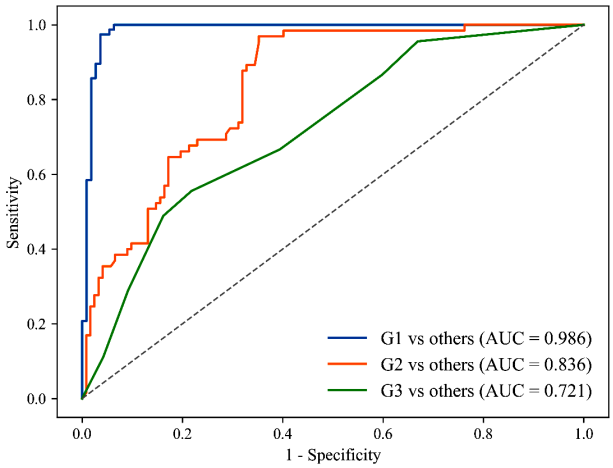

Figure 1. AUC comparison among G1, G2 and G3 vs others.

Table 5. Evaluation of three pathological subtype prediction models.

Model	AUC	Sensitivity	Specificity	Positive prediction value	Negative prediction value
G1 vs Others	0.986 (0.967~ 0.999)	0.974	0.964	0.949	0.981
G1 vs Others	0.836 (0.778~ 0.887)	0.969	0.648	0.594	0.975
G3 vs Others	0.721 (0.638~ 0.799)	0.556	0.782	0.446	0.847

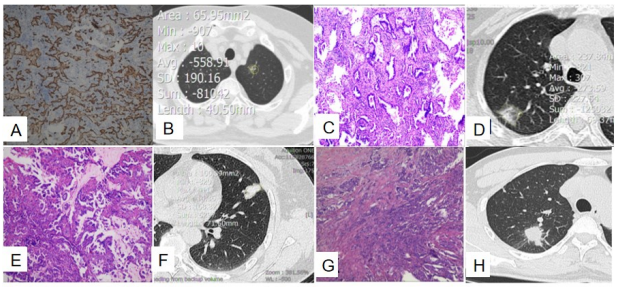

Figure 2. Figures A and B depict a 41-year-old female patient with mixed ground-glass nodules measuring 0.9 x 1.0 cm in the left upper lung, exhibiting an average CT value of -559 Hounsfield units (Hu) and a positive burr sign. Figures C and D illustrate a 63-year-old female patient with mixed ground-glass nodules measuring 1.9 x 1.3 cm in the right upper lung, with an average CT value of -274 Hu, pleural traction, and positive spiculation. Routine pathological examination suggests that the acinar adenocarcinoma is predominantly invasive adenocarcinoma. In Figure E and F, a 73-year-old female patient presented with solid nodules in the left upper lung, measuring approximately 2.5 x 1.7 cm. The nodules exhibited a positive lobulation sign and had an average CT value of 14 Hounsfield units (HU). Pathological analysis identified the nodules as micropapillary-type invasive adenocarcinoma, with cancer metastasis detected in lymph node groups 7 and 11 (3 out of 5 nodes and 2 out of 4 nodes, respectively). In Figure G and H, a 64-year-old male patient exhibited solid nodules in the right upper lung, measuring approximately 2.2 x 1.9 cm, with an average CT value of 73 HU. The nodules were characterized by surrounding spiculation, lobulation, and pleural traction. Pathological examination indicated a solid-based adenocarcinoma, with metastasis to mediastinal lymph node groups 2 and 4 (1 out of 3 nodes and 3 out of 4 nodes, respectively).

DISCUSSION

This study provided valuable evidence supporting the correlation between preoperative CT imaging features and the histopathological subtypes of solitary invasive pulmonary adenocarcinoma. By examining 187 cases stratified into low-risk (G1), intermediate-risk (G2), and high-risk (G3) groups, we identified distinct imaging biomarkers that align closely with the pathological nature of each subtype. The results contribute to a growing effort to integrate imaging with histopathological prediction models for more precise, non-invasive diagnosis and risk assessment in lung cancer.

Our findings confirm that G1 tumors, characterized by lepidic predominance, generally exhibit small size, higher proportions of ground-glass opacity (GGO), and lower CT attenuation values. These features reflect a well-differentiated histological architecture with preserved alveolar structures and minimal stromal invasion. The mean CT value in the G1 group was −486.90 HU, consistent with findings from Ichinose *et al.* [7], who reported that pure ground-glass nodules with low CT values were strongly associated with non-invasive or minimally invasive adenocarcinomas. This radiological phenotype supports the hypothesis that lepidic adenocarcinomas progress slowly and are biologically indolent, making them good candidates for conservative management or sublobar resection.

In contrast, G3 tumors which are dominated by micropapillary and solid histological patterns, showed significantly more aggressive imaging features. These included larger lesion size, increased solid component ratio, and substantially higher CT values, with an average of 52.31 HU. Additionally, G3 tumors frequently demonstrated pleural traction, lobulation, and vascular invasion-signs that are hallmarks of structural distortion and infiltrative behavior. These observations are consistent with previous studies by Yoshida *et al.* [17] and Snoeckx *et al.* [21], who identified solid nodules with high attenuation and architectural irregularities as strong indicators of invasive and high-risk adenocarcinomas. The increased prevalence of spiculation and lobulation in G3 further reinforces the notion that these tumors possess invasive tendencies, potentially extending into surrounding lung parenchyma and pleura.

Intermediate-risk G2 tumors, which included acinar and papillary predominant subtypes, displayed imaging features falling between G1 and G3. While lesion size and CT attenuation were elevated compared to G1, they were lower than those in G3. Interestingly, vascular signs were identified as negative predictors for this group, suggesting that G2 tumors may still preserve some degree of organized vasculature compared to the disrupted microenvironments of G3 tumors. The ability to

[DOI: 10.61882/ijrr.23.3.5]

differentiate G2 from both G1 and G3 on imaging is critical, given the variability in prognosis and recurrence patterns among these subtypes.

The pattern of vascular invasion and air cavity dissemination (STAS) seen in the G3 group underscores the biological aggressiveness of these subtypes. In our study, STAS was observed in 82.2% of G3 tumors compared to just 1.3% in G1. This observation is in line with findings by Shiono *et al.* [22] and Wang *et al.* [23], who emphasized the clinical importance of STAS in predicting poor prognosis and increased recurrence following limited surgical resection. Micropapillary components, in particular, are known for their tendency to detach and spread through air spaces, creating a challenge for complete resection and highlighting the need for more radical surgical approaches such as lobectomy in these cases [24].

It is worth noting that vacuole signs and bronchial signs did not differ significantly across the subtypes. This aligns with prior research suggesting that while these signs may indicate necrosis or bronchiolar involvement, they are not specific enough to differentiate histological subtypes [25]. Their lack of predictive value further emphasizes the need to focus on structural and compositional features-such as lesion size, GGO proportion, spiculation, and pleural traction-when assessing tumor subtype preoperatively.

Our logistic regression models yielded promising results. The G1 model, incorporating lesion size, GGO proportion, CT attenuation, and the burr sign, demonstrated excellent predictive capability (AUC=0.986). This underscores the potential for CT imaging to serve as a non-invasive diagnostic tool, reducing the need for invasive biopsy procedures in patients with radiologically indolent tumors. The G2 model also achieved a respectable AUC of 0.836, while the G3 model, although slightly lower (AUC=0.721), still provided clinically useful discrimination based on lobulation, pleural traction, and female gender. These results are aligned with the trend toward radiomic stratification in oncology, where imaging features can provide surrogate markers for tumor biology and prognosis [26-28].

Furthermore, gender emerged as a significant predictor in the G3 model, with female patients more frequently presenting with high-risk subtypes. This aligns with previous studies, which documented sex-based differences in lung cancer histology, possibly influenced by hormonal, genetic, or environmental factors [29]. Recognizing such demographic patterns could enhance the personalization of lung cancer screening and treatment protocols.

The integration of these imaging markers into clinical decision-making has considerable implications. For example, accurate preoperative identification of lepidic adenocarcinoma could justify the use of limited resection in patients with comorbidities or poor pulmonary reserve. Conversely, detection of features suggestive of micropapillary or solid components might prompt more aggressive surgical management, such as lobectomy or extended lymph node dissection, even in tumors measuring ≤3.0 cm.

This study has a few noteworthy limitations. First, its retrospective and single-center design may introduce selection bias and limit the generalizability of the findings to broader patient populations. Second, while CT features were reviewed by experienced radiologists, the analysis did not incorporate advanced radiomic techniques or artificial intelligence tools, which may have improved the objectivity and predictive performance of the models. Third, the relatively small number of high-risk (G3) cases may limit the statistical power for this subgroup and affect the robustness of the associated predictive model. Lastly, the absence of long-term clinical follow-up restricts our ability to assess the prognostic significance of the imaging features in terms of recurrence, metastasis, and overall survival. Future prospective, multi-center studies with larger cohorts and outcome data are recommended to validate and expand upon these findings.

CONCLUSION

Preoperative CT imaging features show significant correlation with histopathological subtypes of solitary invasive pulmonary adenocarcinoma. Specific CT markers such as ground-glass component, lesion size, CT value, and morphological signs, can reliably predict tumor subtype. These imaging predictors offer valuable non-invasive tools for risk stratification and may inform surgical planning and prognostic assessment in early-stage lung adenocarcinoma.

ACKNOWLEDGMENTS

The authors gratefully acknowledge the support of the Department of Thoracic Surgery and Radiology at the General Hospital of Western Theater Command.

***Funding*:** This study was supported by the Natural Science Foundation of Sichuan Province from the Department of Science and Technology of Sichuan Province (Grant No. 2023NSFSC0721).

***Conflicts of interest*:** The authors declare that there is no conflict of interest regarding the publication of this paper.

***Ethical consideration*:** This research was approved by the Institutional Ethics Committee of the Western Theater Command General Hospital (Approval No. WTCGH/EC/2020-0143). All procedures were conducted in accordance with the Declaration of Helsinki. Patient data were anonymized to protect privacy.

[DOI: 10.61882/ijrr.23.3.5]

Authors' contributions: S.C.: Study design, data collection, draft writing; T.G.: CT image evaluation and analysis; L.Z.: Pathological assessment, interpretation, and final manuscript approval; Y.Z.: Statistical analysis, predictive modeling, co-corresponding author; F.L.: Literature review, figure preparation, manuscript editing.

REFERENCES

1. Zhang Y, Vaccarella S, Morgan E, Li M, Etxeberria J, Chokunonga E, *et al.* (2023) Global variations in lung cancer incidence by histological subtype in 2020: a population-based study. *Lancet Oncol,* ***24*** *(11): 1206-18.*
2. Tan N, Li Y, Ying J, Chen W (2024) Histological transformation in lung adenocarcinoma: Insights of mechanisms and therapeutic windows. *J Transl Int Med,* ***12****(5): 452-65.*
3. Seguin L, Durandy M, Feral CC (2022) Lung Adenocarcinoma Tumor Origin: A Guide for Personalized Medicine. *Cancers (Basel),* ***14*** *(7): 1759.*
4. Rafique M, Manzoor N, Rahman S, Rahman S, Rajput M (2012) Assessment of lung cancer risk due to indoor radon exposure in inhabitants of the state of Azad Kashmir; Pakistan. *Int J Radiat Res,* ***10*** *(1): 19-29*
5. Kolb T, Müller S, Möller P, Barth TFE, Marienfeld R (2024) Molecular heterogeneity in histomorphologic subtypes of lung adeno carcinoma represents a challenge for treatment decision. *Neoplasia, 49: 100955.*
6. Chen C, Chen G, Fang R, Xu Y, Liu H, Liao Z. A New hybrid radiotherapy technique for non-small cell lung cancer: Is more effective for functional lung sparing. International Journal of Radiation Research. 2024;22(3):609-16.
7. Tang Y, He Z, Zhu Q, Qiao G (2014) The 2011 IASLC/ATS/ERS pulmonary adenocarcinoma classification: a landmark in personalized medicine for lung cancer management. *J Thorac Dis,* ***6****(Suppl 5): S589-96.*
8. Travis WD, Brambilla E, Noguchi M, Nicholson AG, Geisinger KR, Yatabe Y, *et al.* (2011) International association for the study of lung cancer/american thoracic society/european respiratory society international multidisciplinary classification of lung adenocarcinoma. *J Thorac Oncol,* ***6****(2): 244-85.*
9. Cao Y, Zhu LZ, Jiang MJ, Yuan Y (2016) Clinical impacts of a micropapillary pattern in lung adenocarcinoma: a review. *Onco Targets Ther,* ***9****: 149-58.*
10. Kadota K, Villena-Vargas J, Yoshizawa A, Motoi N, Sima CS, Riely GJ, *et al.* (2014) Prognostic significance of adenocarcinoma in situ, minimally invasive adenocarcinoma, and nonmucinous lepidic predominant invasive adenocarcinoma of the lung in patients with stage I disease. *Am J Surg Pathol,* ***38****(4): 448-60.*
11. Chae EJ, Song JW, Krauss B, Song KS, Lee CW, Lee HJ, *et al.* (2010) Dual-energy computed tomography characterization of solitary pulmonary nodules. *J Thorac Imaging,* ***25****(4): 301-10.*
12. Rubin GD (2015) Lung nodule and cancer detection in computed tomography screening. *J Thorac Imaging,* ***30****(2): 130-8.*
13. Wu H, Zhang X, Zhong Z (2025) Exploration of CT-based discrimination and diagnosis of various pathological types of ground glass nodules in the lungs. *BMC Med Imaging,* ***25****(1): 119.*
14. Gao JW, Rizzo S, Ma LH, Qiu XY, Warth A, Seki N, *et al.* (2017) Pulmonary ground-glass opacity: computed tomography features, histopathology and molecular pathology. *Transl Lung Cancer Res,* ***6*** *(1): 68-75.*
15. Luo W, Ren Y, Liu Y, Deng J, Huang X (2024) Imaging diagnostics of pulmonary ground-glass nodules: a narrative review with current status and future directions. *Quant Imaging Med Surg,* ***14****(8): 6123 -46.*
16. Ichinose J, Kawaguchi Y, Nakao M, Matsuura Y, Okumura S, Ninomiya H, *et al.* (2020) Utility of maximum CT value in predicting the invasiveness of pure ground-glass nodules. *Clinical lung cancer,* ***21*** *(3): 281-7.*
17. Yoshida Y, Nitadori J-i, Shinozaki-Ushiku A, Sato J, Miyaji T, Yamaguchi T, *et al.* (2017) Micropapillary histological subtype in lung adenocarcinoma of 2 cm or less: impact on recurrence and clinical predictors. *General Thoracic and Cardiovascular Surgery,* ***65****: 273-9.*
18. World Medical Association Declaration of Helsinki (2013) Ethical principles for medical research involving human subjects. *JAMA,* ***310****(20): 2191-4.*
19. Eguchi T, Kadota K, Park BJ, Travis WD, Jones DR, Adusumilli PS (2014) The new IASLC-ATS-ERS lung adenocarcinoma classification: what the surgeon should know. *Semin Thorac Cardiovasc Surg,* ***26*** *(3): 210-22.*
20. Travis WD, Brambilla E, Nicholson AG, Yatabe Y, Austin JHM, Beasley MB, *et al.* (2015) The 2015 World Health Organization Classification of Lung Tumors: Impact of Genetic, Clinical and Radiologic Advances Since the 2004 Classification. *J Thorac Oncol,* ***10*** *(9): 1243-60.*
21. Snoeckx A, Reyntiens P, Desbuquoit D, Spinhoven MJ, Van Schil PE, van Meerbeeck JP, *et al.* (2018) Evaluation of the solitary pulmonary nodule: size matters, but do not ignore the power of morphology. *Insights Imaging,* ***9****(1): 73-86.*
22. Shiono S, Endo M, Suzuki K, Yanagawa N (2020) Spread through air spaces affects survival and recurrence of patients with clinical stage IA non-small cell lung cancer after wedge resection. *J Thorac Dis,* ***12****(5): 2247-60.*
23. Wang Y, Lyu D, Fan L, Liu S (2023) Advances in the prediction of spread through air spaces with imaging in lung cancer: a narrative review. *Transl Cancer Res,* ***12****(3): 624-30.*
24. Eguchi T, Kameda K, Lu S, Bott MJ, Tan KS, Montecalvo J, *et al.* (2019) Lobectomy is associated with better outcomes than sublobar resection in spread through air spaces (STAS)-positive T1 lung adenocarcinoma: a propensity score–matched analysis. *Journal of Thoracic Oncology,* ***14****(1): 87-98.*
25. Health Commission Of The People's Republic Of China N (2022) National guidelines for diagnosis and treatment of lung cancer 2022 in China (English version). *Chin J Cancer Res,* ***34****(3): 176-206.*
26. Wang JH, Wahid KA, van Dijk LV, Farahani K, Thompson RF, Fuller CD (2021) Radiomic biomarkers of tumor immune biology and immunotherapy response. *Clin Transl Radiat Oncol,* ***28****: 97-115.*
27. Reginelli A, Nardone V, Giacobbe G, Belfiore MP, Grassi R, Schettino F, *et al.* (2021) Radiomics as a new frontier of imaging for cancer prognosis: a narrative review. *Diagnostics (Basel),* ***11*** *(10): 1796.*
28. Fusco R, Granata V, Setola SV, Trovato P, Galdiero R, Raso MM, *et al.* (2025) The application of radiomics in cancer imaging with a focus on lung cancer, renal cell carcinoma, gastrointestinal cancer, and head and neck cancer: A systematic review. *Physica Medica,* ***130****: 104891.*
29. May L, Shows K, Nana-Sinkam P, Li H, Landry JW (2023) Sex differences in lung cancer. *Cancers (Basel),* ***15****(12): 3111.*

[DOI: 10.61882/ijrr.23.3.5]